peaks at 330, 354, 405, 460, and 573 nm clearly correspond to the ultraviolet peaks of $C_{76}$ at 329, 354 (sh), 405, 452 (sh), and 574 nm (*16*), establishing that the CD spectra correspond to resolved $C_{76}$. The kinetically resolved $C_{76}$ after 95% conversion showed an optical rotation $[\alpha]_D$ of −4000° (concentration: 0.0034, in toluene). The starting material analyzed after 33% conversion showed 28% of this optical activity. These two points in the relationship between optical activity and conversion in the kinetic resolution allowed calculation of the enantiomeric excess of the recovered starting material (*17*); the recovered $C_{76}$ after 95% conversion is >97% enantiomeric excess. The maximum specific rotation of $C_{76}$ is estimated to be 4000 ± 400° at the sodium *D*-line, a value comparable with the helicenes (*18*).

The differences between the enantiomers of $C_{76}$ are not immediately obvious from molecular models. However, when you constrain your view to a particular type of bond, such as the site of greatest local curvature (bond 5), the differences become clearer (Fig. 4). This exercise has implications at the molecular level. Resolution techniques which interact with $C_{76}$ molecules over their entire surface, such as chiral stationary-phase HPLC, manifest little difference between the enantiomers and ineffective resolution. However, resolution techniques which selectively operate upon a particular part of $C_{76}$, such as regioselective asymmetric osmylation, have a much better chance of enantiomer discrimination. For example, the approach to bond 5 in Fig. 4 shows that the van der Waals surface curves away from this probable main reaction site with very different handedness for the two enantiomers. Chiral recognition may involve diastereotopic attractive π-π interactions between the phenanthryl units of $\mathbf{L}^1$ and $\mathbf{L}^2$ and these contoured fullerene surfaces (*19*, *20*). This technology could be applied to the resolution of other chiral fullerenes.

### REFERENCES AND NOTES


1. R. Ettl, I. Chao, F. Diederich, R. L. Whetten, *Nature* **353**, 149 (1991).
2. F. Diederich and R. L. Whetten, *Acc. Chem. Res.* **25**, 119 (1992).
3. J. M. Hawkins, A. Meyer, T. A. Lewis, S. Loren, F. J. Hollander, *Science* **252**, 312 (1991).
4. J. M. Hawkins, *Acc. Chem. Res.* **25**, 150 (1992).
5. ______, S. Loren, A. Meyer, R. Nunlist, *J. Am. Chem. Soc.* **113**, 7770 (1991).
6. J. M. Hawkins *et al.*, *ibid.* **114**, 7954 (1992).
7. J. M. Hawkins, A. Meyer, M. A. Solow, unpublished results.
8. J. M. Hawkins, A. Meyer, M. Nambu, in preparation.
9. For example, see V. S. Martin *et al.*, *J. Am. Chem. Soc.* **103**, 6237 (1981).
10. K. B. Sharpless *et al.*, *J. Org. Chem.* **56**, 4585 (1991).
11. K. B. Sharpless *et al.*, *ibid.* **57**, 2768 (1992).
12. J. R. Colt and G. E. Scuseria, *J. Phys. Chem.* **96**, 10265 (1992).
13. R. C. Haddon, *Acc. Chem. Res.* **21**, 243 (1988).
14. As with $C_{70}$, the bonds between the most pyramidalized carbons in $C_{76}$ are not the shortest bonds.
15. Small quantities of $C_{76}$ were measured spectrophotometrically.
16. The UV spectrum of $C_{76}$ in toluene is similar to the published spectrum in $CH_2Cl_2$ (*1*). The shoulder at 452 nm in $CH_2Cl_2$ is not well defined in toluene, so the value from $CH_2Cl_2$ is listed.
17. A. R. Schoofs and J.-P. Guetté, in *Asymmetric Synthesis*, J. D. Morrison, Ed. (Academic Press, New York, 1983), vol. 1, chap. 3.
18. K. P. Meurer and F. Vögtle, in *Topics in Current Chemistry*, F. L. Boschke, Ed. (Springer-Verlag, New York, 1985), vol. 127, pp. 32–53.
19. Chiral recognition in the asymmetric bisosmylation of $C_{60}$ appears to be governed by attractive interactions (*8*).
20. Regeneration of $C_{76}$ separately from the two major isomers of $C_{76}(OsO_4py_2)$ will indicate whether the chiral recognition mechanisms for the two major reaction paths are additive or partially subtractive.


21. We thank N. Holden for a generous loan of fullerene extract, G. Scuseria for his calculated coordinates of $C_{76}$, R. Haddon for a copy of his POAV analysis program, S. Loren and T. Robinson for computer expertise, Regis Chemical Company for a complementary Buckyclutcher I column, and K. B. Sharpless for chiral ligand samples. J.M.H. is grateful to NSF (Presidential Young Investigator Award, CHE-8857453), DOE, the Camille and Henry Dreyfus Foundation (Teacher-Scholar Award), Merck Sharp & Dohme Research Laboratories, the Shell Oil Company Foundation, Xerox Corporation, Monsanto Company, Hoffmann-La Roche Inc., Chevron Research and Technology Company, and Eli Lilly and Company for financial support.

30 March 1993; accepted 5 May 1993


# Evidence from Western North America for Rapid Shifts in Climate During the Last Glacial Maximum


Bruce D. Allen and Roger Y. Anderson



**The Estancia basin in southwestern United States contains evidence for strong and rapid pulsations in the supply of moisture brought into the region during the last ice age. The pulses were recorded during episodes of stream discharge that spread plumes of fresh water laden with quartz sand over the saline lake. The largest pulses in stream discharge lasted only a few decades, were organized into cycles that were spaced approximately 200 to 250 and 2000 years apart, and were of sufficient magnitude to freshen and maintain the lake at its maximum recorded elevation.**


When the last great ice sheet was nearing collapse, high-latitude regions may have warmed by as much as 7°C within 40 to 50 years (*1*). In Greenland, the quantity of dust trapped in ice and the isotopic composition of the ice changed dramatically in less than 20 years (*1*, *2*). Evidence for rapid shifts in climate comes from sites above 65°N, and little is known about sudden changes in climate in the region that lies to the south of the Laurentide ice sheet. In this report we describe evidence for large and equally rapid changes in precipitation from pluvial Lake Estancia, central New Mexico, 35°N, 106°W (Fig. 1A).

Today, the floor of Estancia basin is occupied by numerous playas. During the last glacial maximum and deglaciation, a greatly expanded Lake Estancia experienced two major highstands, one beginning ~19,700 years ago and another ~13,700 years ago (Table 1). The early highstand formed the highest shoreline at 1890 m, at which time the lake had a surface area of 1100 $km^2$ and a water depth of 45 m. The high ratio of lake surface area to drainage area (Fig. 1B) produced large fluctuations in water volume and hydrochemistry as a result of changes in precipitation and evaporation. The absence of glaciers in the upland drainage means that recharge was entirely from precipitation, direct runoff, and ground water, with no lag effects from melting ice.

The fauna preserved in Estancia sediment consists largely of calcareous valves of ostracodes. Two species, *Limnocythere staplini* and *Candona rawsoni*, are present throughout most of the lake sequence. Other species, including *Cytherissa lacustris*, *Candona caudata*, and *Limnocythere ceriotuberosa*, are restricted to narrow stratigraphic zones throughout the central area of the basin and were used to correlate between localities.

By tracing lowstand strata to their shoreline elevation, we determined that groundwater discharge had maintained a minimum pool of ~400 $km^2$ throughout the period of deglaciation until ~12,000 years ago. The continuity of centimeter-scale layers of sediment and faunal zones over distances of several kilometers in the area once covered by the permanent pool indicates that accumulation was continuous and that the basin contains an uninterrupted record of climate variability.

Age control for changes within the glacial maximum highstand (gmh) sequence (~20,000 to ~15,000 years ago) is provided by radiocarbon dates of various organic


Department of Earth and Planetary Sciences, University of New Mexico, Albuquerque, NM 87131.

fractions collected from the lake sediments (Table 1). Because all of the dated materials are aquatic in origin, the chronology may be biased from a hardwater effect of unknown magnitude. However, the large ratio of surface area to volume of Lake Estancia probably facilitated exchange between atmospheric $CO_2$ and dissolved carbon in the lake, which would have minimized the hardwater effect (3). Depth of bioturbation in the gmh sequence, as indicated by the small size of burrows and by preservation of delicate color banding, was generally <1 cm. Dated units are from several localities, and the correlation of strata between localities was established with the use of ostracode zones.

Lake sediments that accumulated during the gmh are exposed in natural excavations (wind blowouts) in the central area of the basin and consist largely of marly clay containing varying amounts of sand- and silt-sized gypsum. To find evidence for changes

**Table 1.** Radiocarbon dates referenced in the text and in Fig. 1D. The earliest date marks the beginning of the second major highstand of Lake Estancia. Dates are conventional $^{14}C$ years before the present. Error values (in parentheses) are $1\sigma$.

| Date | Laboratory | Material dated |
|---|---|---|
| 13700 (105) | AA 6327 | Ostracode valves |
| 16310 (240) | Beta 33737 | Disseminated organics |
| 17160 (210) | Beta 33362 | Disseminated organics |
| 18730 (550) | W 5484 | Disseminated organics |
| 19760 (160) | AA 6329 | Ostracode valves |
| 20040 (240) | AA 1867 | *Ruppia* seeds |

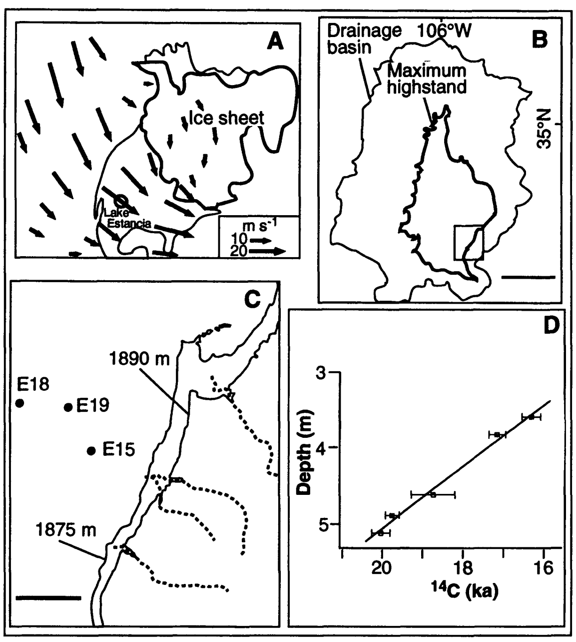


**Fig. 1.** (**A**) Location of Lake Estancia in relation to a generalized depiction of simulated winds aloft (~500 mbar) in January during last glacial maximum [adapted from (*10*)]. Arrows are wind vectors. (**B**) Map of Estancia basin showing the large surface area of the lake relative to that of the drainage basin. Scale bar, 20 km. (**C**) Stream channels terminating at the gmh. Streams discharged clastic sediment, including sand-sized grains of detrital quartz, directly into the saline lake. Dotted lines represent truncated streams. Scale bar, 3 km. (**D**) Age model showing distribution of radiocarbon dates versus depth at locality E19; ka = thousand years ago.

in climate, we examined the stratigraphic record exposed in three natural excavations at localities E15, E18, and E19 (Fig. 1C). The gmh sequence was sampled at contiguous 2.5-cm intervals and analyzed for carbonate and gypsum content, species abundance of adult ostracodes, and abundance of detrital quartz grains. The abundance of quartz grains per gram of lake sediment was determined from grain counts of the sieved fraction that were >250 μm. High sediment accumulation rates (~40 cm per 1000 years), the radiocarbon age model (Fig. 1D), and minimal bioturbation provide a resolution of ~60 years per 2.5-cm sample.

Detrital quartz was concentrated in narrow stratigraphic intervals at each of the three localities. A shoreward source for the detrital quartz grains was identified by measurement of their abundance in the same stratigraphic unit (*C. lacustris* zone) at distances that were progressively farther from the highstand shoreline (Fig. 1C). The size and abundance of detrital quartz across this transect decrease with increasing distance from the shore (Fig. 2A). We believe that the detrital quartz was carried in runoff and streamflow and was flushed into the lake during the gmh by streams that entered the lake along its southeastern shore (Fig. 1C). Transport of sand toward the center of the basin can be explained by the formation of plumes of sediment-laden fresh water that spread over the more saline and dense water that occupied the basin before an episode of streamflow. This interpretation is supported by observations of modern freshwater sediment plumes. In Pyramid Lake, Nevada, for example, a layer of fresh water from spring snowmelt was observed to spread above saline lake water, and the plume carried clastic grains in the same size range as those found at Estancia more than 4 km from the point of discharge (4).

Stream channels preserved along the southeastern shore (Fig. 1C) and elsewhere around the margin of the lake terminate abruptly at the maximum highstand shoreline (1890 m); less developed channels extend to a slightly lower highstand (~1880 m). The truncated channels demonstrate that significant stream discharge occurred only during full-lake conditions and that little or no streamflow occurred thereafter. An uninterrupted proxy of streamflow was reconstructed from detrital quartz at site E19 for the entire duration of glacial-maximum conditions, from ~20,000 to ~15,000 years ago (Fig. 2B). Streamflow events are spaced ~200 to 250 years apart and are grouped into longer, millennial cycles with maxima separated by ~2000 years.

Pulses in stream discharge identified by thin zones of detrital quartz were found to be synchronous with abrupt changes in the

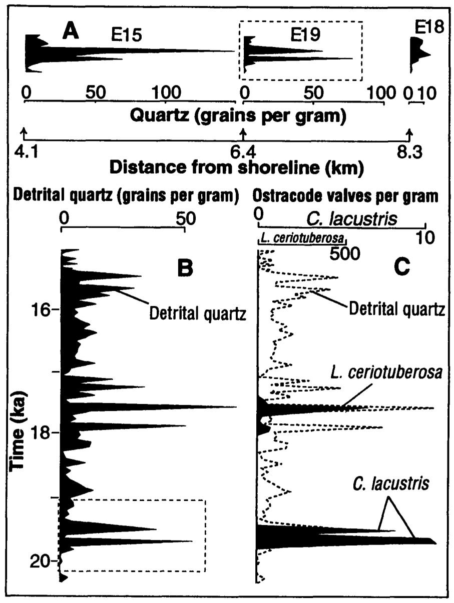


**Fig. 2.** (**A**) Transect showing decrease in abundance of detrital quartz with increasing distance from glacial-maximum shoreline. Detrital quartz probably was carried toward the center of the basin in sediment plumes discharged by streams along the southeast shore (see Fig. 1C for transect localities relative to stream channels). (**B**) Changes in abundance of detrital quartz at locality E19 throughout the gmh of Lake Estancia. Peaks in the abundance of detrital quartz, a proxy for episodes of streamflow, are separated by several hundred years and are grouped into longer, ~2000-year oscillations. Area outlined by the dashed line corresponds to that in (A). (**C**) Abundance of *C. lacustris* and *L. ceriotuberosa* relative to incursions of detrital quartz. Changes in ostracode species abundance (freshening events) coincide with maxima in detrital quartz abundance (streamflow events).

abundance of species of ostracodes that are sensitive to changes in hydrochemistry (*5*, *6*). For example, peaks in abundance of *C. lacustris*, which is found today only in lakes with low values of total dissolved solids (TDS) [<500 mg liter$^{-1}$ (*5*)], coincide with the two discharge events that marked the initial rise toward the gmh ~19,700 years ago (Fig. 2C). The appearance of *C. lacustris* in the same 2.5-cm sample as the first quartz peak indicates that the lake freshened within a few decades of the onset of stream discharge. The presence of this *C. lacustris* zone throughout the center of the basin, even in areas that lie beyond the apron of detrital quartz distributed by sediment plumes, shows that episodes of runoff freshened the entire lake.

Growth pulses of other species of ostracodes are also associated with detrital quartz peaks, but these species tolerate a wider range of salinity than does *C. lacustris* and also may be linked to specific anions. For example, peaks in the abundance of *L. ceriotuberosa*, which is sensitive to anion composition (*6*), are coincident with a second group of peaks in quartz abundance, after ~18,000 years ago (Fig. 2C). Other species with wider TDS ranges than *C. lacustris*, including *C. caudata* and *C. rawsoni*, also responded during episodes of streamflow.

Mass balance calculations (*7*) in conjunction with the age model (Fig. 1D) were used in the estimation of changes in lake level and TDS during episodes of streamflow. Because of its known association with low TDS (*5*), *C. lacustris* was used to constrain the amount of freshening and to estimate rates of runoff during the rise in lake level at the onset of the gmh. We used empirically derived values of precipitation (53 cm year$^{-1}$) and evaporation (66 cm year$^{-1}$) for the Estancia basin during the glacial maximum (*8*), which take into consideration the effect that reduced temperatures, on the basis of snow line–depression data, might have had on evaporation rates. These are crude estimates at best but sufficient for the estimation of temporal changes in TDS and provide a frame of reference with previous studies at Lake Estancia (*8*, *9*). We calculated the time required, under glacial-maximum conditions, to reduce TDS from 8000 mg liter$^{-1}$ [the species-estimated value (*7*) before the freshening event ~19,700 years ago] to 500 mg liter$^{-1}$ (the value required to support a population of *C. lacustris*).

When rates of runoff are <~25% of precipitation over the drainage basin, stream discharge is insufficient to reduce TDS to a concentration that supports *C. lacustris* within the time constraint of several decades. With no discharge from streams, the lake never reaches the elevation of the highstand shorelines (Fig. 3), and with 5% runoff ~200 years is required to achieve enough freshening to support a population of *C. lacustris*. Although we made several simplifying assumptions, changing the input values within reasonable limits does not alter our conclusion that Lake Estancia was freshened and rose to highstands as a result of major episodes of increased runoff and stream discharge that lasted no more than a few decades.

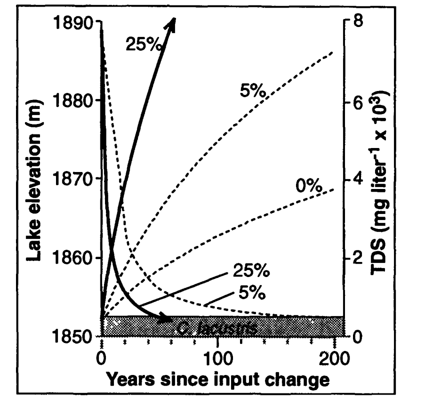


**Fig. 3.** Output from model simulation at several rates of runoff (indicated by percent values), showing changes in lake level for glacial-maximum estimates of precipitation and evaporation (*8*). Also illustrated are changes in concentration (TDS) during simulated episodes of 25% and 5% runoff. The elevation of the gmh and a TDS value capable of supporting *C. lacustris* are reached within the time constraint of a few decades only with significant runoff.

Rapid decreases in ostracode abundance after major episodes of runoff and freshening indicate an abrupt end to streamflow and a rapid return to higher TDS values. For example, *C. caudata* has an optimal TDS value of ~2000 mg liter$^{-1}$ (*5*) and grew rapidly during the two episodes of freshening that began ~19,700 years ago. Abundance of *C. caudata* decreased sharply within decades (an interval of one 2.5-cm sample) after the second discharge event. A fivefold change in the value for precipitation minus evaporation, coupled with the cessation of stream discharge, is needed to drive concentrations above 2000 mg liter$^{-1}$ and to exceed the optimal TDS value for *C. caudata* within the necessary time frame.

Under modern conditions, surface runoff in the Estancia basin rarely reaches the valley floor, and recharge to the modern playas is almost entirely by ground water. Well-developed stream channels ending at the high shoreline are physical evidence that precipitation and runoff were important contributions to lake recharge during the gmh. With the estimate of 53 cm year$^{-1}$ for annual precipitation (*8*) used in our calculations, a 25% runoff coefficient implies an increase in precipitation of ≥13 cm year$^{-1}$. This value is a minimum estimate of change in precipitation during rapid shifts in climate because some unknown fraction of the actual increase was lost to infiltration and evapotranspiration.

Moisture entrained from the Pacific Ocean is the likely source of much of the precipitation that fell on the Estancia basin during the gmh. A general circulation model for 18,000 years ago (*10*), for example, depicts a maximum in wind velocity aloft south of the Laurentide ice sheet and directs the strongest zonal flow into the continental interior at about the latitude of Estancia basin (Fig. 1A). The simulated regional temperature at 18,000 years ago (*10*) is consistent with winter snowfall and spring snowmelt, conditions that would have contributed to strong spring runoff and to the observed distribution of detrital quartz grains in lake sediments.

Large changes in water balance (highstands and lowstands) observed in other pluvial lakes in western North America have been attributed to changes in precipitation and evaporation that were associated with changes in the position of the polar-front jet stream (*11*). Such a mechanism might help to explain some of the changes in climate at the Estancia site. However, major highstands at Estancia, beginning ~19,700 and ~13,700 years ago, appear to coincide, within the accuracy of dating, with glacial advances in both hemispheres (*12*). This timing suggests that the major changes in climate recorded at Lake Estancia were part of a global as well as a regional response.

The evidence from Estancia further shows that millennial-scale oscillations in moisture occurred as several strong pulses in precipitation that lasted only a few decades and were separated by a few hundred years (Fig. 2B). The amplitude of these decadal shifts in climate support an inference that the changes in the transport of water vapor across the continent were an aspect of the rapid reorganizations in climate that have been identified at high latitudes (*1*, *2*, *13*) and that characterize the last glacial maximum and its transitions.

## REFERENCES AND NOTES


1. W. Dansgaard, J. W. C. White, S. J. Johnson, *Nature* **339**, 532 (1989).
2. K. Taylor, R. Alley, G. Lamorey, *Eos* **73**, 259 (1992).
3. J. V. Turner, P. Fritz, P. F. Karrow, B. G. Warner, *Can. J. Earth Sci.* **20**, 599 (1983).
4. R. Y. Anderson, *Limnol. Oceanogr.* **22**, 423 (1977).
5. L. D. Delorme, *Geosci. Can.* **16**, 85 (1989).
6. R. M. Forester, *Geology* **14**, 796 (1986).
7. The hydrologic balance was calculated in annual steps with the equation $dV/dt = (P - E) \times A + GWD + R$ where $V$ is lake volume, $P$ is annual precipitation, $E$ is annual evaporation, $A$ is lake area; $GWD$ is annual ground-water discharge, and $R$ is annual surface runoff. Leakage of ground water was assumed to be negligible compared to other terms in the mass balance equation over the annual step size. With regard to the removal of dissolved solids in the salt balance calculations, we considered only deposition of calcium carbon-

ate and calcium sulfate, on the basis of analyses of contiguous sediment samples. Depth and surface area were recalculated for each step with morphometric data for the basin. The initial lake elevation before the rise during the glacial maximum was 1852 m, on the basis of shoreline gravels linked to basin-center stratigraphy. Before the rise in elevation, TDS was set to 8000 mg liter$^{-1}$, which is somewhat lower than previously estimated for this unit by F. W. Bachhuber [*Geol. Soc. Am. Bull.* **101**, 1543 (1989)]. This lower TDS value was chosen as a conservative estimate of runoff and corresponds to the upper part of the optimal range for *C. rawsoni* [D. R. Engstrom and S. R. Nelson, *Palaeontol. Palaeoolimnol. Palaeoceanogr.* **83**, 295 (1991)], which is present in small numbers in this interval. The TDS in runoff from snowmelt and streamflow was set to 100 mg liter$^{-1}$, about half the concentration in five modern spring-fed streams in the upland drainage In ground water, TDS was set to 2100 mg liter$^{-1}$, on the basis of an average of five water wells nearest the zone of ground-water discharge. The ground-water discharge rate was set to $1.25 \times 10^8$ m$^3$ year$^{-1}$. This value was reached on the basis of the average rate of accumulation of calcium carbonate and calcium sulfate in the lake bed and on the assumption that there is a long-term balance between the input of dissolved solids in ground water and their removal to sediments. This value is on the same order of magnitude as an estimate of ground-water discharge for the modern hydrologic system by B. E. DeBrine [thesis, New Mexico Institute of Mining and Technology (1971)].

8. L. B. Leopold, *Am. J. Sci.* **219**, 152 (1951).
9. E. Antevs, *J. Geol.* **62**, 182 (1954).
10. J. E. Kutzbach and H. E. Wright, *Quat. Sci. Rev.* **4**, 147 (1985).
11. S. Hostetler and L. E. Benson, *Clim. Dyn.* **4**, 207 (1990).
12. W. S. Broecker and G. H. Denton, *Geochim. Cosmochim. Acta* **53**, 2465 (1989).
13. P. M. Grootes and M. Stuiver, *Eos* **73**, 258 (1992).
14 We thank F. W. Bachhuber for providing several radiocarbon dates and L. V. Benson and P. De Deckker for comments. Supported by National Science Foundation grant EAR-9019134.

21 December 1992; accepted 23 March 1993

# Spatiotemporal Patterns in the Energy Release of Great Earthquakes

Barbara Romanowicz

**For the past 80 years, the energy released in great strike-slip and thrust earthquakes has occurred in alternating cycles of 20 to 30 years. This pattern suggests that a global transfer mechanism from poloidal to toroidal components of tectonic plate motions is operating on time scales of several decades. The increase in seismic activity in California in recent years may be related to an acceleration of global strike-slip moment release, as regions of shear deformation mature after being reached by stresses that have propagated away from regions of great subduction decoupling earthquakes in the 1960s.**

The contributions of toroidal and poloidal components of global tectonic plate motions are about equal (*1*). The poloidal component, associated with upwelling and downwelling currents, is directly related to density variations in the deep mantle. The toroidal component, which represents horizontal shearing, exists primarily because of the presence of the rigid lithospheric plates and the associated heterogeneity in rheology. In addition to aseismic motions, which are difficult to observe, the poloidal component is expressed in thrust and normal faulting and the toroidal one, in strike-slip earthquakes. Yet the temporal pattern of seismic energy release is dominated by that of great thrust earthquakes, which are more than one order of magnitude larger than the largest strike-slip earthquakes. The contribution of the latter has therefore largely been ignored in analyses of temporal patterns of global seismic moment release.

In this report, I examine the spatiotemporal distribution of great shallow earthquakes since 1920 by taking into account the fault geometry and, as a first approximation, by considering two classes of earthquakes separately: strike-slip and subduction zone thrust earthquakes. Data are taken from the CMT (Centroid Moment Tensor) catalog (*2*) for the past 15 years, as well as from catalogs of great earthquakes in the last century (*3, 4*) and a recently published catalog of large earthquakes by Pacheco and Sykes (PS) (*5*).

Seismographic Station and Department of Geology and Geophysics, University of California, Berkeley, CA 94720.

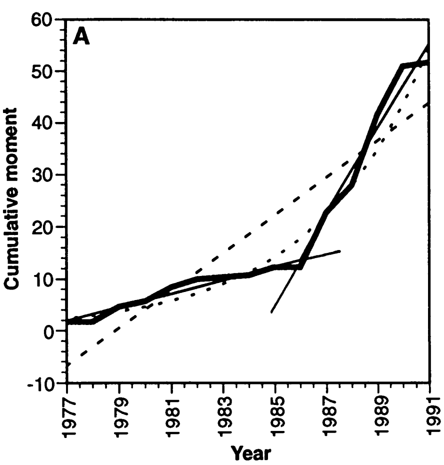


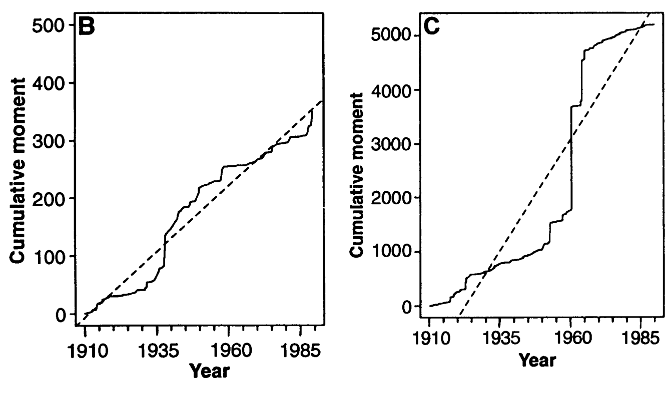


**Fig. 1.** (**A**) Cumulative moment released by strike-slip earthquakes in the past 15 years, from the CMT catalog (*2*). In all figure parts, the units of cumulative moment are $10^{20}$ N-m. The calculation is done with a yearly increment. All strike-slip earthquakes of moment larger than $0.1 \times 10^{20}$ N-m have been included, where strike-slip is defined as corresponding to a mechanism with minimum dip of both nodal planes of 55°. The results are robust with respect to changes by 5° to 10° in this definition. For reference, the best fitting linear curve (dashed line) and the best fitting exponential curve (dotted line), where $\Sigma M = M_0\, e^{+t/\tau}$, are shown; the rise time $\tau$ for the exponential fit is about 5 years. If we remove the Macquarie Island earthquake of 23 May 1989 from consideration, the rise time remains ~5 years. Also shown are separate linear fits for the periods 1977 to 1986. (**B**) Cumulative moment release by strike-slip earthquakes in the PS catalog (*5*). (**C**) Same as (B) for non–strike-slip earthquakes. Note the change of scale from (B) to (C). Most of the great strike-slip earthquakes would disappear into the background if both types of earthquakes were plotted together.

The total seismic energy release is dominated by that of the largest or "great" earthquakes (*3, 6*). The temporal and spatial patterns observed for these earthquakes are different and more regular than those of moderate to large ones. Several interesting temporal patterns have been recognized. In the record of the past 50 years, a striking feature is a peak in the earthquake energy release around 1960 (*3*) when several great earthquakes occurred within a few years. This peak is correlated with a peak in the amplitude of the Chandler wobble, although the physical connection between these two phenomena is still a matter of debate (*7–10*). Another feature is the progression of great earthquakes around both the Pacific rim and the Alpide Belt between 1935 and 1965 (*11*). The total energy